Large-eddy simulations of a forced homogeneous isotropic turbulence with polymer additives*

Wang Lu(王 璐), Cai Wei-Hua(蔡伟华), and Li Feng-Chen(李凤臣)†

School of Energy Science and Engineering, Harbin Institute of Technology, Harbin 150001, *China*

(Received 16 June 2013; revised manuscript received 21 July 2013; published online 14 January 2014)

Large-eddy simulations (LES) based on the temporal approximate deconvolution model were performed for a forced homogeneous isotropic turbulence (FHIT) with polymer additives at moderate Taylor Reynolds number. Finitely extensible nonlinear elastic in the Peterlin approximation model was adopted as the constitutive equation for the filtered conformation tensor of the polymer molecules. The LES results were verified through comparisons with the direct numerical simulation results. Using the LES database of the FHIT in the Newtonian fluid and the polymer solution flows, the polymer effects on some important parameters such as strain, vorticity, drag reduction, and so forth were studied. By extracting the vortex structures and exploring the flatness factor through a high-order correlation function of velocity derivative and wavelet analysis, it can be found that the small-scale vortex structures and small-scale intermittency in the FHIT are all inhibited due to the existence of the polymers. The extended self-similarity scaling law in the polymer solution flow shows no apparent difference from that in the Newtonian fluid flow at the currently simulated ranges of Reynolds and Weissenberg numbers.

Keywords: forced homogeneous isotropic turbulence, polymer additives, large-eddy simulation, temporal approximate deconvolution model

PACS: 47.27.Gs, 47.50.–d, 47.27.ep **DOI:** 10.1088/1674-1056/23/3/034701

1. Introduction

The phenomenon that adding a minute amount of long-chain polymers or some kinds of surfactants to water or organic solvent flows can induce an obvious turbulent drag reduction (DR) was firstly reported by Toms (Toms' effect[1]). This phenomenon has been extremely attractive since its discovery due to the prospect of saving energy. It is repeatedly found that there exists a dramatic frictional DR in the pipe and channel turbulent flows of polymer or surfactant solution,[2,3] and the DR rate can reach even more than 80% in some situations.[4] Therefore, the drag-reducing effect has great potential in the practical application systems. For example, in a district heating/cooling system, it can lead to the decrease of the pipe diameter, an increase of the flow rate, a reduction of pumping power energy consumption, and so on.

In order to get an insight into the mechanism of the turbulent DR, a large amount of studies have been carried out both experimentally and numerically. By experimental efforts, the rheological properties of the viscoelastic polymer or surfactant solutions, the topological characteristics of microstructures in the solutions under shear, the overall DR feature and its influencing factors, the statistical and structural characteristics of the turbulent velocity fields, and convective heat transfer behaviors in polymer or surfactant solution flows have been successfully obtained.[5–13]

However, due to the limitations in even up-to-date experimental techniques, the *in-situ* measurements of the conformation field of microstructures (structured by either polymer molecules in polymer solution or micelles formed by surfactant molecules in surfactant solution) and the elastic stress field in the viscoelastic fluid flow are unavailable as yet, which are the key parameters (interacting with the turbulence) for exploring the mechanism of DR. Therefore, numerical simulations are relied on for the purpose of obtaining thorough information, including the microstructure conformation and elastic stress fields as well as the velocity field in turbulent drag reducing flows.

The direct numerical simulation (DNS) can resolve the dissipation scale in a turbulent flow, so it should be the best numerical simulation method for any turbulent flows including the drag-reducing flow of viscoelastic fluid provided that the computer can be powerful enough. Indeed, the DNS method has been used in many studies to resolve the detailed characteristics of drag-reduced turbulent flows and investigate the mechanism of DR.[14–20] However, high spatial and temporal resolutions are necessary for the DNS of a turbulent flow to resolve the dissipation scale, resulting in extremely large computational consumptions, which is unaffordable for the current computers if the flow Reynolds number is as high as that

*Project supported by the National Natural Science Foundation of China (Grant Nos. 51206033 and 51276046), the Specialized Research Fund for the Doctoral Program of Higher Education of China (Grant No. 20112302110020), the China Postdoctoral Science Foundation (Grant No. 2011M500652), the Heilongjiang Postdoctoral Science Foundation, China (Grant No. 2011LBH-Z11139), and the Natural Scientific Research Innovation Foundation in Harbin Institute of Technology, China (Grant No. HIT.NSRIF.2012070).

†Corresponding author. E-mail: lifch@hit.edu.cn

© 2014 Chinese Physical Society and IOP Publishing Ltd

in most industrial application systems. Therefore, the DNS approach is not suitable for the computation of engineering problems. In practical engineering fields, Reynolds averaged Navier–Stokes (RANS) models are commonly used to simulate complex turbulent flows. The idea of the RANS approach is to establish turbulence models to represent the relations between high-order and low-order statistics. So far, several RANS models have been proposed for the turbulent drag-reducing flow of viscoelastic fluid. For example, Cruz and Pinho[21] presented a low Reynolds number k–ε turbulence model for a turbulent drag-reducing fluid pipe flow. It was observed that this model can capture the dissipation rate away from the wall, however the turbulent kinetic energy obtained with this model deviates from the experimental results. Cruz *et al.*[22] proposed a two-equation k–ε turbulence model for the turbulent pipe flow of viscoelastic fluid, which can adequately predict the turbulent kinetic energy. Nevertheless, the quantitative information from the RANS approach is limited (only mean values of turbulence parameters are available).

In the 1970s, the large-eddy simulation (LES) method was proposed, which makes up for the disadvantages of DNS and RANS. Since the LES resolves turbulence eddies at scales above a threshold length scale and models eddies below this threshold scale, it can thus not only reduce the computation burden compared with the DNS but also obtain more information of the micro-scaled turbulent flow parameters than the RANS. With these unique advantages, the LES has been widely used in scientific and engineering fields to compute turbulent flows at high Reynolds numbers. The principal work for the LES is to establish a suitable subgrid-scale (SGS) model, which is derived from the interactions between unresolved-scale and resolved-scale structures and represents the effect of the unresolved-scale structures on the resolved-scale structures. Up to now, many SGS models have been proposed, such as Smagorinsky's model,[23] the dynamic model,[24] and the mixed model.[25] These models have been widely used in the simulations of the turbulent channel, pipe, and some complicated geometrical flows of Newtonian fluids.

Domaradzki and Saiki[26] presented a velocity estimation model, which substitutes the unfiltered velocity field by the deconvolution of the filtered velocity field to estimate the SGS stress. This idea is based on the fact that the filtering operation can be expressed as an invertible form when the polynomials of the inverses reach a certain degree. Considering the repeated applications of the approximate deconvolution of the filtered data by the truncated expansions of the inverse filtering operation, Stolz and Adams[27] came up with the approximate deconvolution model (ADM), which was used to simulate both incompressible and compressible fluids' wall-bounded flows.[28,29] In addition to the excellent LES results obtained using the ADM, the computation cost is less than that of the dynamic model and the velocity estimate model. It was also suggested by Pruett[30] that the filtering approach can be based on both space domain and time domain, which is called the temporal LES. Relative to spatial filters, temporal filters have many advantages, such as, the independence of the simulation grid for implicit methods and the accordance with the process of the experiment. Taking into account the idea of a temporal filter in addition to the ADM, Pruett *et al.*[31] proposed a temporal approximate deconvolution model (TADM), which is proved to be comparable with the fully resolved DNS (mean streamwise velocity in wall units, Reynolds stress etc). The computation requirement for the TADM is inevitably higher than that for the ADM because of the larger storage of variable values in the TADM. Recently, Thais *et al.*[32] first attempted to perform the LES for a turbulent drag-reducing channel flow of viscoelastic fluid using the TADM. They confirmed that the TADM is able to exactly express the residual stress. Moreover, they also presented the relationships between the Reynolds stress and the temporal filter width, the ensemble-averaged mean and root-mean-square fluctuations of conformation tensor, and the influence of the filter width on those parameters. However, detailed information in the viscous sub-layer was not discussed.

On the other hand, research on drag-reducing viscoelastic fluid flows so far have focused on the wall turbulence, such as pipe and channel flow, boundary layer flow, and swirling flow in a cylindrical container. The existence of the wall can easily arouse non-uniformity in turbulence, which brings about difficulties in the analysis of the interactions between molecular micro-structures and turbulence structures in viscoelastic fluid flows. The wall effect is eliminated in homogenous isotropic turbulence (HIT) or grid turbulence. There have been a few important results by the DNS and experiments on the HIT or grid turbulence in viscoelastic fluid flows.[33–37] However, as mentioned above, the DNS has its limitations in computing flows at high Reynolds number.

In this paper, we report one of our continuous numerical studies on the drag-reducing turbulent flow of viscoelastic fluid. Forced HIT (FHIT) in viscoelastic polymer solution is chosen in order to eliminate the wall effect. The LES is performed for the FHIT in viscoelastic fluid based on the TADM. The finitely extensible nonlinear elastic in the Peterlin approximation (FENE-P) model is adopted as the constitutive equation for the filtered conformation tensor of polymer molecules. The present study has two main purposes. The first one is to do another test on the TADM-based LES of turbulence in viscoelastic fluid flow by choosing FHIT without the wall effect in addition to the TADM-based LES of wall turbulence as originally performed by Thais *et al.*[32] After establishing a reliable LES method using the TADM for drag-reducing FHIT, the second purpose is to investigate the statistical characteris-

tics of the FHIT with polymer additives at elevated Reynolds number (still moderate range though), as compared with our previous DNS studies on low Reynolds number HIT of viscoelastic fluid flow.[38] In Section 2, we show the detailed governing equations of the TADM for viscoelastic fluid flows and the calculation conditions. In Section 3, our in-house code is at first validated for the Newtonian fluid and the polymer solution flow cases. Then the characteristics of FHIT influenced by viscoelastic polymer additives at moderate Reynolds number are discussed in detail. Conclusions drawn from this study are given in Section 4.

2. Governing equations and calculation conditions

2.1. Governing equations

2.1.1. Continuity and modified momentum equations

The continuity and the modified momentum equations for the LES of FHIT with polymer additives based on the TADM are as follows:[32]

$$\frac{\partial \overline{u}_i}{\partial x_i} = 0, \tag{1}$$

$$\begin{aligned}\frac{\partial \overline{u}_i}{\partial t} + \overline{u_j}\frac{\partial \overline{u_i}}{\partial x_j} = &-\frac{1}{\rho}\frac{\partial \overline{p}}{\partial x_i} + \upsilon^{[s]}\frac{\partial^2 \overline{u}_i}{\partial x_j x_j} + \upsilon^{[s]}\frac{1-\beta}{\beta}\frac{\partial \overline{T}^{[p]}_{ij}}{\partial x_j} \\ &- \frac{\partial M_{ij}}{\partial x_j} + \chi_u\left(\overline{w_i} - \overline{u_i}\right) \\ &+ \upsilon^{[s]}\frac{1-\beta}{\beta}\frac{\partial R_{ij}}{\partial x_j} + f_i,\end{aligned} \tag{2}$$

where $\overline{u}_i(x_i,t)$ is the filtered velocity; $\overline{p}(x_i,t)$ is the filtered local pressure; ρ is the solution density; $\beta = \upsilon^{[s]}/(\upsilon^{[s]}+\upsilon^{[p]})$ is a dimensionless measurement of the dilute polymer solution concentration and a smaller β corresponds to a denser polymer solution, here $\upsilon^{[s]}$ is the solvent viscosity, and $\upsilon^{[p]}$ is the polymeric zero-shear-rate viscosity (if $\beta = 1.0$, Eq. (2) is the filtered momentum equation for the FHIT of the Newtonian fluid); $\overline{T}^{[p]}_{ij} = (f(\overline{r})\overline{C}_{ij} - 1)/\tau_p$ is the filtered elastic stress, here $\overline{C}_{ij}$ is the filtered conformation tensor; τ_p is the polymer relaxation time; $f(\overline{r}) = (l^2-3)/(l^2-\overline{r}^2)$ ensures the finite extensibility, with l being the maximum chain extensibility; $\overline{r}^2$ is the trace operator, $\overline{r}^2 = \mathrm{trace}(\overline{C}_{ij})$; M_{ij} is the modeled residual Newtonian stress obtained by deconvolving the resolved-scale velocity field; χ_u is the dissipative coefficient for the momentum equation and $\chi_u = 1$ for this study; R_{ij} is a subfilter term related to the nonlinear restoring force; and f_i is the external force.

In order to obtain M_{ij} and the dissipative regularization term $\chi_u(\overline{w_i} - \overline{u_i})$, the deconvolved velocity v_i and w_i is defined to approximate the unresolved-scale u_i. So v_i, M_{ij}, and w_i are modeled as[32]

$$v_i = \sum_{m=0}^{p} C_m \overline{u}_i^{(m+1)}, \tag{3}$$

$$M_{ij} = \overline{v_i v_j} - \overline{v}_i \overline{v}_j, \tag{4}$$

$$w_i = \sum_{m=0}^{q} D_m \overline{u}_i^{(m+1)}. \tag{5}$$

The filtering method of the TADM for the momentum equation is as follows:[32]

$$\frac{\partial \overline{u}_i^{(m+1)}}{\partial t} = \frac{\overline{u}_i^{(m)} - \overline{u}_i^{(m+1)}}{\Delta_u}, \quad 1 \le m \le \max(p,q), \tag{6a}$$

$$\frac{\partial \overline{v}_i}{\partial t} = \frac{v_i - \overline{v}_i}{\Delta_u}, \tag{6b}$$

$$\frac{\partial \overline{v_i v_j}}{\partial t} = \frac{v_i v_j - \overline{v_i v_j}}{\Delta_u}, \tag{6c}$$

$$\frac{\partial \overline{w}_i}{\partial t} = \frac{w_i - \overline{w}_i}{\Delta_u}, \tag{6d}$$

where Δ_u is the filter width for the momentum equation. The initial conditions for the velocity filtering are $\overline{u_i}(0,x) = \overline{u_i}^{(2)}(0,x) = \overline{u_i}^{(3)}(0,x) = \overline{u_i}^{(4)}(0,x) = u_i(0,x)$, $\overline{v_i}(0,x) = \overline{w_i}(0,x) = u_i(0,x)$, and $\overline{v_i v_j}(0,x) = u_i u_j(0,x)$.

In this study, we use degree-3 deconvolution for p and degree-2 secondary regularization for q, i.e., $p = 3$ and $q = 2$. According to the binomial theorem, the optimal deconvolution coefficients are $[C_0, C_1, C_2, C_3] = [0, \sqrt{6}, \sqrt{4+2\sqrt{6}} - 2\sqrt{6}, 1 - \sqrt{4+2\sqrt{6}} + \sqrt{6}]$ and $[D_0, D_1, D_2] = [15/8, -9/8, 1/4]$.[31]

2.1.2. Conformation tensor transport equation

The conformation tensor transport equation using the Dumbbell model[39] for the FHIT of polymer solution flow for the LES based on the TADM is given by

$$\begin{aligned}&\frac{\partial \overline{C_{ij}}}{\partial t} + \overline{u_k}\frac{\partial \overline{C_{ij}}}{\partial x_k} \\ &= \overline{C_{ik}}\frac{\partial \overline{u_j}}{\partial x_k} + \overline{C_{kj}}\frac{\partial \overline{u_i}}{\partial x_k} + P_{ij} + Q_{ij} - R_{ij} + \chi_c(\overline{\gamma_{ij}} - \overline{C_{ij}}) \\ &\quad - \frac{1}{\tau_p}\left[\alpha f(\overline{r})\overline{C_{ik}C_{kj}} + (1-\alpha)f(\overline{r})\delta_{ik}\overline{C_{kj}}\right. \\ &\quad \left. - \alpha\overline{C_{ik}}\delta_{kj} - (1-\alpha)\delta_{ij}\right],\end{aligned} \tag{7}$$

where P_{ij} and Q_{ij} are the subfilter terms caused by stretching; R_{ij} is a subfilter term related to the nonlinear restoring force, which is the same as that in the momentum equation; χ_c is the dissipative coefficient for the conformation tensor transport equation and $\chi_c = 1$ for this study; α is the mobility factor; and δ_{ij} is the Kronecker mark.

For the sake of gaining subfilter terms and the second order regularization term $\chi_c(\overline{\gamma_{ij}} - \overline{C_{ij}})$, the deconvolution conformation tensors ϕ_{ij} and γ_{ij} which represent the approximation of the unfiltered conformation tensor are built as[32]

$$\phi_{ij} = \sum_{m=0}^{p} C_m \overline{C}_{ij}^{(m+1)}, \tag{8}$$

$$\gamma_{ij} = \sum_{m=0}^{q} D_m \overline{C}_{ij}^{(m+1)}, \tag{9}$$

where p and q are the same as those used in the momentum

equation, $p=3$ and $q=2$; and the coefficients C_m and D_m are also consistent with those in the momentum equation.

Then the subfilter terms P_{ij} and Q_{ij} are built from the deconvolution velocity v_i and the deconvolution conformation tensor ϕ_{ij} as[32]

$$P_{ij}=\overline{\frac{\partial v_i}{\partial x_k}\phi_{kj}}-\frac{\partial \overline{v}_i}{\partial x_k}\overline{\phi}_{kj}, \tag{10}$$

$$Q_{ij}=\overline{\frac{\partial v_j}{\partial x_k}\phi_{ki}}-\frac{\partial \overline{v}_j}{\partial x_k}\overline{\phi}_{ki}. \tag{11}$$

The R_{ij} exists in both the momentum equation and the conformation tensor transport equation. For this subfilter term, a deconvolution elastic stress T_{ij} is defined to approximate the unfiltered elastic stress[32]

$$T_{ij}=\frac{f(\phi)\phi_{ij}-1}{\tau_{\rm p}}, \tag{12}$$

$$R_{ij}=\overline{T}_{ij}-\frac{f(\overline{\phi})\overline{\phi}_{ij}-1}{\tau_{\rm p}}. \tag{13}$$

The filter of the variables above is also based on the time domain[32]

$$\frac{\partial \overline{C}_{ij}^{(m+1)}}{\partial t}=\frac{\overline{C}_{ij}^{(m)}-\overline{C}_{ij}^{(m+1)}}{\Delta_{\rm c}},\quad 1\le m\le \max(p,q), \tag{14a}$$

$$\frac{\partial \overline{\phi}_{ij}}{\partial t}=\frac{\phi_{ij}-\overline{\phi_{ij}}}{\Delta_{\rm c}}, \tag{14b}$$

$$\frac{\partial \overline{\gamma}_{ij}}{\partial t}=\frac{\gamma_{ij}-\overline{\gamma_{ij}}}{\Delta_{\rm c}}, \tag{14c}$$

$$\frac{\partial}{\partial t}\left(\overline{\frac{\partial v_i}{\partial x_k}\phi_{kj}}\right)=\frac{1}{\Delta_{\rm c}}\left(\frac{\partial v_i}{\partial x_k}\phi_{kj}-\overline{\frac{\partial v_i}{\partial x_k}\phi_{kj}}\right), \tag{14d}$$

$$\frac{\partial}{\partial t}\left(\overline{\frac{\partial v_j}{\partial x_k}\phi_{ki}}\right)=\frac{1}{\Delta_{\rm c}}\left(\frac{\partial v_j}{\partial x_k}\phi_{ki}-\overline{\frac{\partial v_j}{\partial x_k}\phi_{ki}}\right), \tag{14e}$$

$$\frac{\partial \overline{T_{ij}}}{\partial t}=\frac{T_{ij}-\overline{T_{ij}}}{\Delta_{\rm c}}, \tag{14f}$$

where $\Delta_{\rm c}$ is the filter width for the conformation tensor transport equation. It is worth mentioning that it is not necessary for $\Delta_{\rm c}$ to be equal to Δ_u. The initial conditions for the conformation tensor filtering are $\overline{C_{ij}}(0,x)=\overline{C_{ij}}^{(2)}(0,x)=\overline{C_{ij}}^{(3)}(0,x)=\overline{C_{ij}}^{(4)}(0,x)=C_{ij}(0,x)$, $\overline{\phi_{ij}}(0,x)=\overline{\gamma_{ij}}(0,x)=C_{ij}(0,x)$, and $\overline{T_{ij}}(0,x)=T_{ij}(0,x)$.

The velocity field and the conformation tensor field can be obtained by solving the coupled Eqs. (1), (2), and (7).

2.2. Computational model and related conditions

2.2.1. Computational model

In this paper, we use a periodic cubic domain of size $R=2\pi$ cm with 32^3 and 64^3 collocation points. A standard pseudo-spectral code is programmed. For Eq. (2), 3/2 rule is adopted to eliminate the aliasing error caused by the pseudo-spectral. In order to maintain the symmetrically positive definite of the conformation tensor, a second order Kurganov–Tadmor scheme[40] is used for the convective term in Eq. (7). For other terms in Eq. (7), a second order central difference scheme is employed. In both the momentum and the conformation tensor transport equations, a second order Adams–Bashforth scheme is adopted for time marching, and a second order Runge–Kutta scheme is used for filtering on the time domain.[32]

2.2.2. External forcing

In order to obtain the statistically stationary variables, an external force is added in Eq. (2) to the large scales to maintain the turbulence. The substance of the external force is to keep the largest scales' energy constant. There are many kinds of methods to realize the addition of the external force. In this paper, the realization method of external force proposed by Chen *et al.*[41] is chosen for both the Newtonian fluid and the polymer solution cases. This method states that the total energy in each of the first two wavenumber shells ($1\le k<2$ and $2\le k<3$) is maintained invariant in time evolution. Therein, the energy spectrum is expressed as[41]

$$E(k)=\sum\nolimits_{S(k)}\left|u(k')\right|^2/2, \tag{15}$$

where $S(k)$ is the computational domain in the shell; and $\sum_{S(k)}$ is the energy in one wavenumber shell ($k\le|k'|<k+1$). For keeping the energy constant, the energies with $E_1=0.305684$ and $E_2=0.130452$ are injected into the first and the second wavenumber shells, respectively. For each time step, by solving the momentum equation without the external force in spectral space, we obtain the velocity $u_i'(\boldsymbol{k})(t+\delta t)$. Then by means of multiplying $u_i'(\boldsymbol{k})(t+\delta t)$ with the wavenumber between $1\le k<2$, the updated velocity can be obtained as follows:[41]

$$\hat{u}_i(\boldsymbol{k})(t+\delta t)=u_i'(\boldsymbol{k})(t+\delta t)\sqrt{E_1/E(1)(t)}, \tag{16}$$

where $\hat{u}_i(\boldsymbol{k})(t+\delta t)$ is the updated velocity field; and $E(1)(t)$ is the total energy for $1\le k<2$ calculated by $u_i'(\boldsymbol{k})(t+\delta t)$. For the velocity field in wavenumber $2\le k<3$, a similar procedure is performed.

2.2.3. Computational cases and parameters

Firstly, we define two important parameters, the Taylor micro-scale Reynolds number Re_λ and the Weissenberg number Wi based on the Newtonian fluid as a reference, which are expressed as

$$Re_\lambda=\frac{\sqrt{20}\xi^{[\rm N]}}{\sqrt{3\upsilon^{[\rm s]}\varepsilon^{[\rm N]}}}, \tag{17a}$$

$$Wi=\tau_{\rm p}\sqrt{\frac{\varepsilon^{[\rm N]}}{\upsilon^{[\rm s]}}}, \tag{17b}$$

where

$$\xi^{[\rm N]}=\frac{1}{2}\langle\overline{u}^2\rangle=\frac{1}{3}\int_0^\infty E(k)\,{\rm d}k,$$

$$\varepsilon^{[\rm N]}=\upsilon^{[\rm s]}\int_0^\infty k^2E(k)\,{\rm d}k$$

are the turbulent kinetic energy and the turbulent energy dissipation rate in the Newtonian fluid flow, respectively. The

initial turbulent kinetic energy spectrum is chosen as $E_0(k) = 0.01k^4\exp(-0.14k^2)$ in this study.

We have simulated the Newtonian fluid and the polymer solution cases with 32^3 and 64^3 collocation points, respectively. The simulation parameters are listed in Table 1. Numerical results for the cases of N1 and V1 with 32^3 collocation points are used for code validation. Results for the remaining cases, N2, V2, and V3, with 64^3 collocation points are utilized for investigating the characteristics of the FHIT.

Table 1. Parameters for all simulations.

Run	l	$\upsilon^{[s]}/\mathrm{cm}^2\cdot\mathrm{s}^{-1}$	τ_p/s	β	Re_λ	Wi
N1	0	10^{-2}	0	1.0	46	0
N2	0	3×10^{-3}	0	1.0	90	0
V1	100	10^{-2}	0.1, 0.2, 0.3, 0.4	0.6, 0.7, 0.8, 0.9	46	0.340
V2	100	3×10^{-3}	0.05	0.6, 0.7, 0.8, 0.9, 0.95	90	0.357
V3	100	3×10^{-3}	0.12	0.8, 0.9, 0.95	90	0.857

3. Results and discussion

Before analyzing the characteristics of the FHIT, the LES code for the Newtonian fluid (Run N1) and the polymer solution (one case in Run V1) flows based on the TADM is validated by comparing the LES results with the DNS results.[38] Under the current simulation conditions, the 32^3 collocation points for LES and the 96^3 collocation points for DNS are comparable, because the Taylor micro-scale Reynolds numbers Re_λ's are the same for the two cases. For the polymer solution case, the flow at $Wi = 0.34$, $\beta = 0.8$ is chosen for comparison. The turbulent kinetic energy spectrum and the probability density function (PDF) of the velocity gradient tensor, which are the two key parameters for the FHIT, obtained by LES and DNS are compared, as shown in Figs. 1 and 2. Due to the isotropy of the FHIT, we just give the PDF of $\partial u/\partial x$. From Fig. 2(a), it can be observed that $E(k)$ stays constant in the small scale range for the polymer solution (compared with $E(k)$ for DNS in Fig. 1(a)), straightforwardly indicating that the turbulent kinetic energy transfer process for the Newtonian fluid has been modified in the FHIT with polymer additives. However, due to the limitation of the simulated grid in LES (32^3), the available wavenumber k cannot reach the extent of that in DNS (96^3) so that the interesting phenomenon ($E(k)$ for DNS in Fig. 2(a)) cannot be captured. Nevertheless, it can be seen that the turbulent kinetic energy spectrum at small wavenumber and the PDF of the velocity gradient tensor show good agreements between LES and DNS results for both the Newtonian fluid and the polymer solution fluid cases. This sufficiently indicates that our LES code using the TADM for the FHIT of the Newtonian fluid and the polymer solution are accurate and reliable. The polymer effect on the turbulent characteristics of the FHIT at moderate Re_λ is then analyzed based on the LES database as follows.

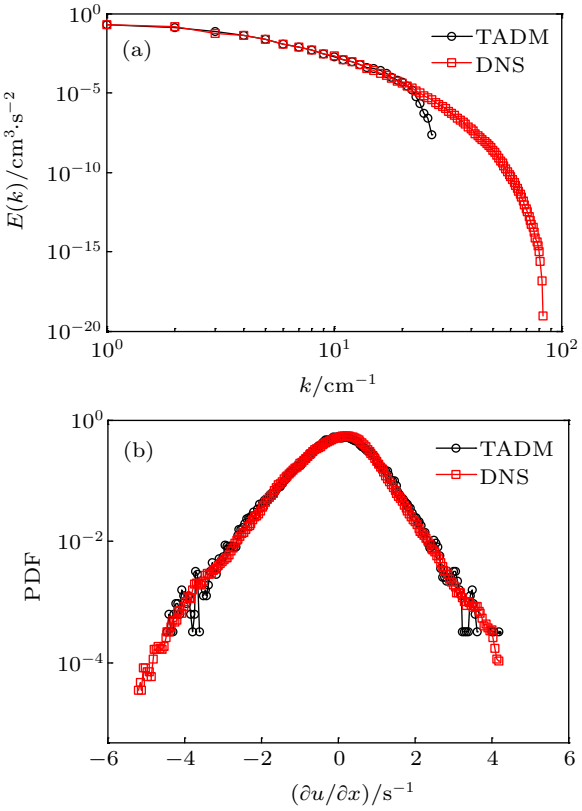


Fig. 1. (color online) (a) Turbulent kinetic energy spectrum at $t = 60$ s; (b) PDF of $\partial u/\partial x$ for the Newtonian fluid flow.

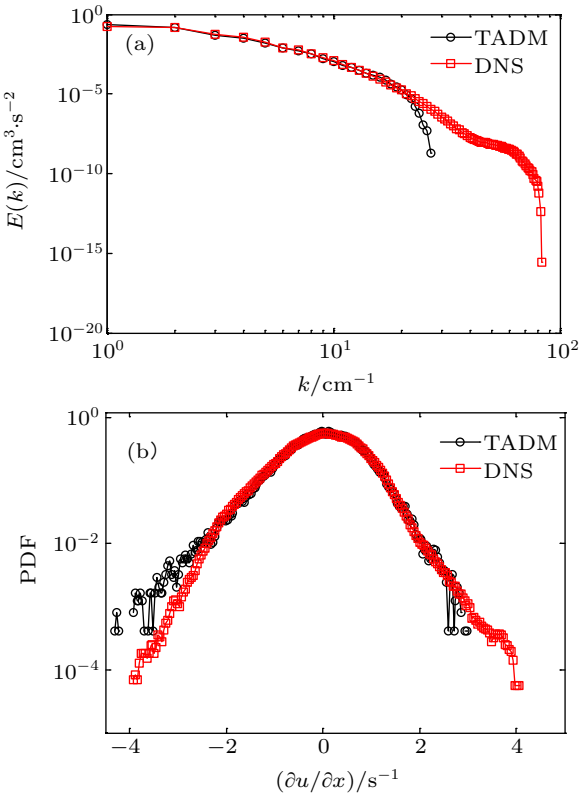


Fig. 2. (color online) (a) Turbulent kinetic energy spectrum at $t = 60$ s; (b) PDF of $\partial u/\partial x$ for polymer solution flow at $Wi = 0.34$, $\beta = 0.8$.

3.1. Statistical characteristics of the FHIT influenced by polymer additives

One of the most important features of the FHIT, as compared to the decaying HIT (DHIT), is that statistically stationary turbulent quantities can be obtained when the numerical simulation on turbulence reaches the statistically stable state.

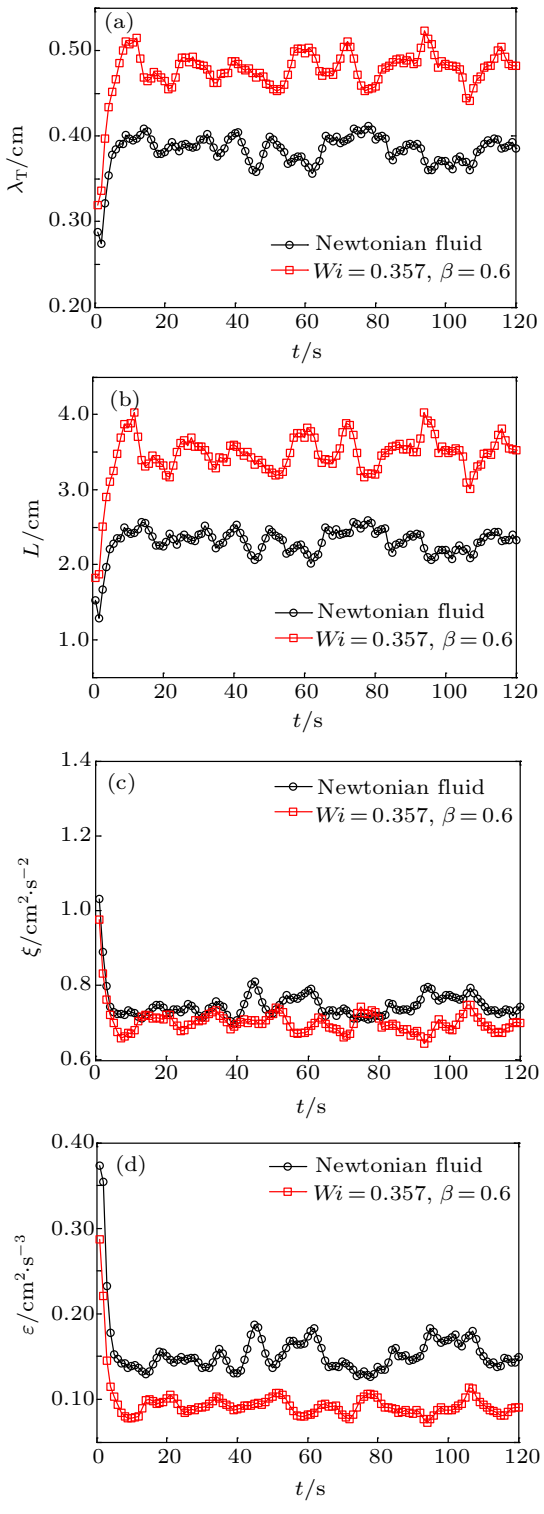


Fig. 3. (color online) Time evolutions of basic parameters: (a) Taylor micro-scale; (b) turbulent integral scale; (c) turbulent kinetic energy; (d) energy dissipation rate.

Based on the LES of the FHIT, we analyze the following turbulent quantities: Taylor micro-scale, turbulent integral scale, turbulent kinetic energy, and energy dissipation rate. The Taylor micro-scale and the turbulent integral scale are defined as $\lambda_T = \sqrt{15\upsilon^{[s]}\langle u^2\rangle/\varepsilon}$ and $L = \langle u^2\rangle^{3/2}/\varepsilon$, respectively. The time evolutions of these four quantities are shown in Fig. 3. It can be seen that λ_T and L first increase and then attain the statistically stable state for both the Newtonian fluid and the polymer solution flows, whereas ξ and ε first decrease and then reach the stable state. Compared with the Newtonian fluid case, λ_T and L are larger, and ξ and ε are lower for the polymer solution case due to the existence of viscoelasticity. All these parameters reach a statistically stable state after $t = 15$ s. In order to study the influence of the polymer solution concentration and Wi on these four quantities, their statistical average values are calculated based on the data from $t = 15$ s to $t = 120$ s, as shown in Fig. 4. It shows that λ_T and L both increase with the decreases of β (increase of the solution concentration) and Wi (Figs. 4(a) and 4(b)); ξ increases with the increase of β and the decrease of Wi (Fig. 4(c)); ε increases with the increase of β but has nonvisible change within the range of simulated Wi (Fig. 4(d)). The increase of L means that the turbulent kinetic energy possessed by the large-scale vortex structures in turbulence is increased, causing the change of the large-scale vortex structures. Along with the increase of the polymer solution concentration, the viscoelasticity effect is more and more intense, leading to the decreases of ξ and ε. This will be elucidated in detail later.

As is known, the velocity gradient tensor is an appropriate parameter used for exploring the kinetic and dynamic characteristics of a turbulence due to its connection with the vortex structures and energy cascade process. The velocity gradient tensor can also be divided into strain and vorticity tensors. First, the time evolutions of strain and vorticity are given in Fig. 5. It is found that both strain and vorticity are lower in the FHIT of the polymer solution than those in the FHIT of the Newtonian fluid caused by the polymer effect. Then we study the impact of β and Wi on the strain and the vorticity, and analyze the PDF, as shown in Figs. 6 and 7. It is shown that the strain and the vorticity have the same decrease tendencies with the decrease of β and the increase of Wi (see Figs. 6(a) and 7(a)). Also, the larger the polymer solution concentration is, the more the PDF distribution of strain moves to the small value of strain (see Fig. 6(b)), indicating that the polymers can reduce the region of large strain and augment the region of small strain. Similar results about the PDF of vorticity can also be found in Fig. 7(b).

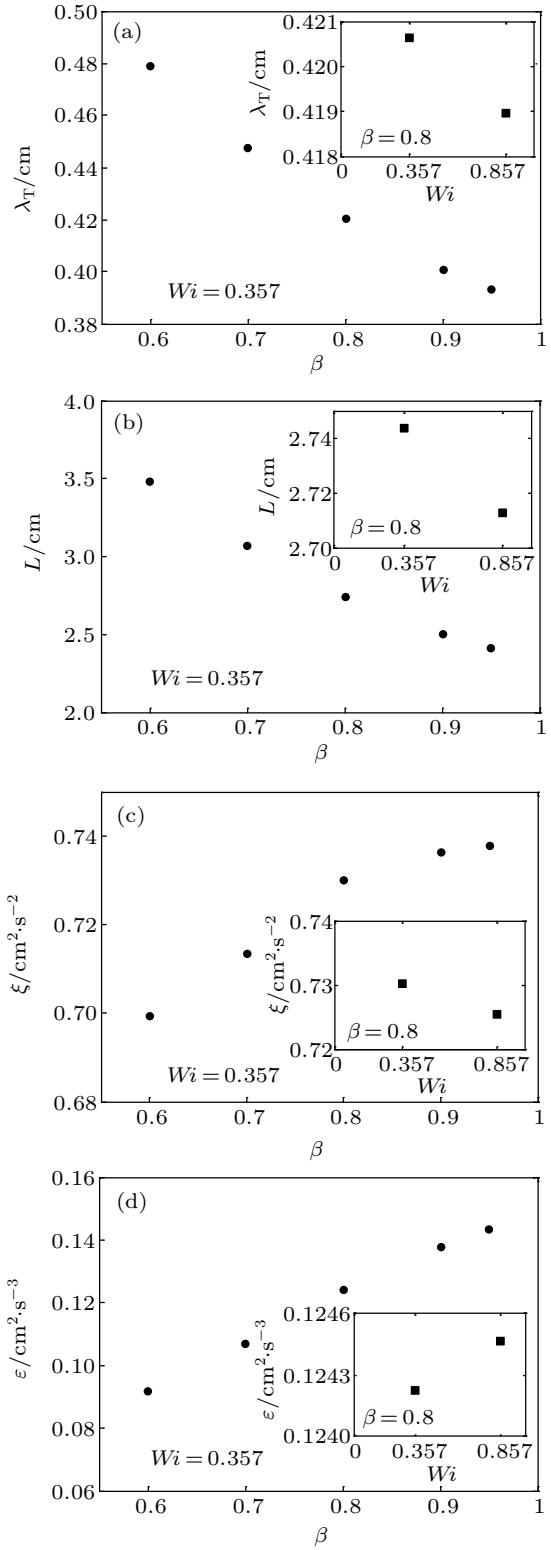


Fig. 4. The influences of β and Wi on basic parameters: (a) Taylor micro-scale; (b) turbulent integral scale; (c) turbulent kinetic energy; (d) energy dissipation rate.

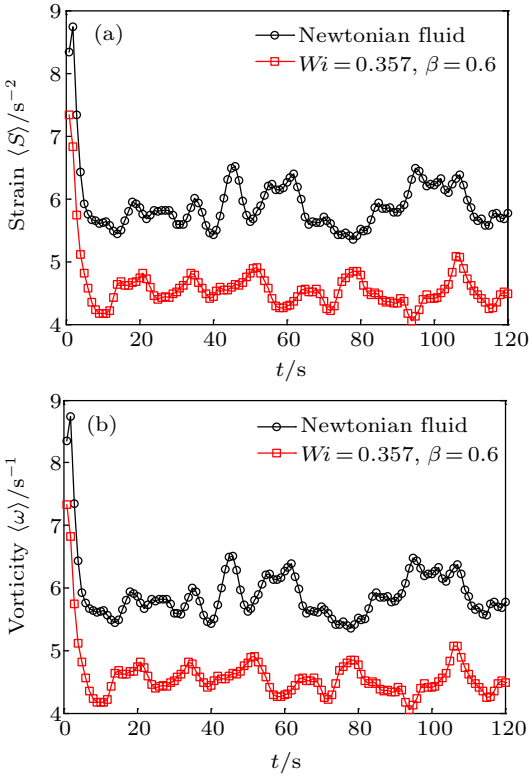


Fig. 5. (color online) Time evolutions of (a) strain and (b) vorticity.

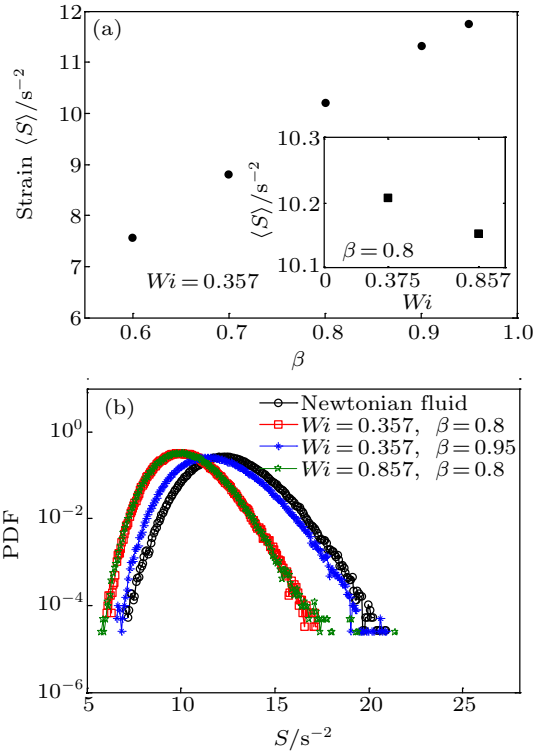


Fig. 6. (color online) The influences of β and Wi on (a) the strain and (b) the PDF of the strain.

As mentioned above, the addition of polymer decreases the turbulent kinetic energy (see Fig. 3(c)). The decreased portion of the turbulent kinetic energy is absorbed by the polymers, causing the decrease of the turbulent energy dissipation rate (see Fig. 3(d)). As analyzed below, the same as that in the DHIT,[37] the turbulent drag-reducing effect by polymer additives also appears in the FHIT without wall shear stress. In our previous study,[37] we proposed a definition of DR for the FHIT of polymer solution

$$\mathrm{DR} = \frac{\Delta\xi^{[\mathrm{p}]} - \Delta\xi^{[\mathrm{N}]}}{\Delta\xi^{[\mathrm{N}]}} \times 100\%, \tag{18}$$

where $\Delta\xi = (\xi_F + \xi_{ini}) - \xi_{eq}$, in which the bracketed term is the total initial turbulent energy including the original added energy ξ_F ($\xi_F = E_1 + E_2$) and the initial turbulence kinetic energy ξ_{ini} ($\xi_{ini} = \sum_k E_0(k)$), and ξ_{eq} is the statistical turbulence kinetic energy at the stable state as shown in Fig. 4(c). The superscript p represents the polymer solution flow. For both the Newtonian fluid and the polymer solution cases, the total initial energy is the same, whereas $\xi_{eq}^{[p]} < \xi_{eq}^{[N]}$, resulting in $\Delta\xi^{[p]} > \Delta\xi^{[N]}$ and a positive DR rate. The definition of DR in this way directly exhibits the ability of the drag-reducing additives in suppressing the turbulence. Figure 8 shows the estimated DR as a function of β and Wi. It can be clearly seen that the DR increases with the increases of the polymer solution concentration (decrease of β) and Wi.

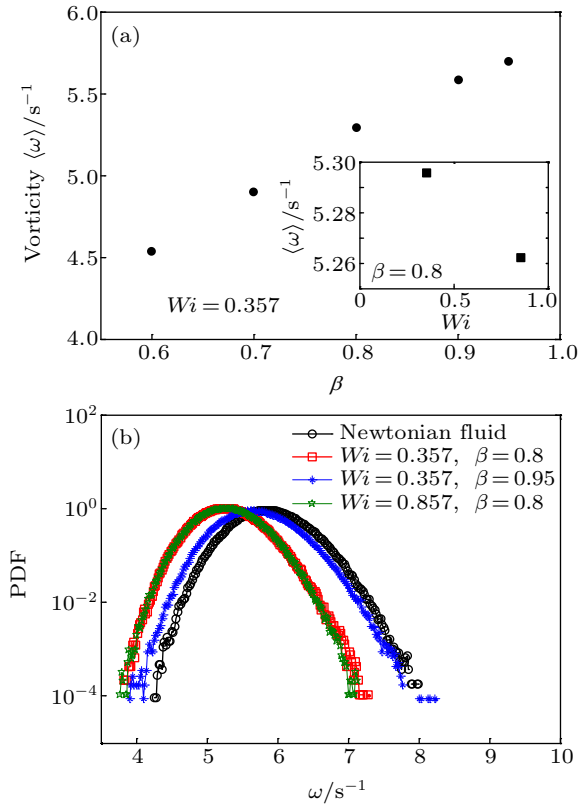


Fig. 7. (color online) The influences of β and Wi on (a) the vorticity and (b) the PDF of the vorticity.

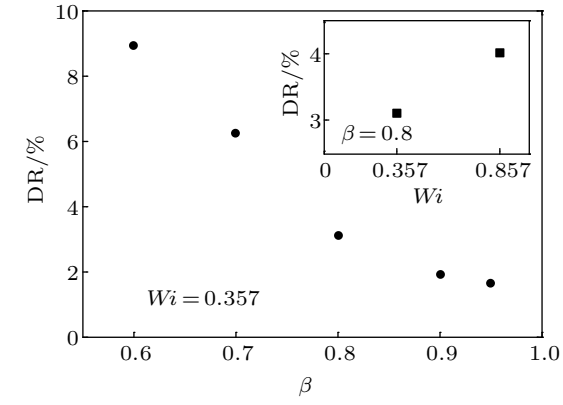


Fig. 8. DR rate versus β and Wi (inset).

3.2. Turbulence coherent structures in FHIT influenced by polymer additives

The extraction of coherent structures for turbulent flows, including both wall-bounded turbulent flow and HIT, has played an important role in understanding the characteristics of the turbulence.[42–45] The turbulence coherent structures can be divided into vortex tubes giving rise to the intermittency and vortex sheets where a large quantity of turbulent kinetic energy dissipates due to the existence of a strong strain. Exploring the characteristics of vortex tube and vortex sheet in the FHIT with polymer additives is of great importance in understanding the mechanism of turbulent DR in viscoelastic fluid flows.

Many methods for extracting the vortex tube have been presented so far. The so-called Q method[46–48] is adopted herein to exact the vortex tube. For the velocity gradient tensor $\nabla \boldsymbol{u}$ of a turbulent flow, the equation of its eigenvalue, λ, is written as

$$\lambda^3 + P\lambda^2 + Q\lambda + R = 0, \tag{19}$$

where P, Q, and R are the three invariants of $\nabla \boldsymbol{u}$, and $P = S_{ii}$, $Q = (P^2 - S_{ij}S_{ji} - W_{ij}W_{ji})/2$, $R = (-P^3 + 3PQ - S_{ij}S_{jk}S_{ki} - 3W_{ij}W_{jk}W_{ki})/3$. Here $S_{ij} = (\partial u_j/\partial x_i + \partial u_i/\partial x_j)/2$ is the strain tensor and $W_{ij} = (\partial u_j/\partial x_i - \partial u_i/\partial x_j)/2$ is the vorticity tensor. For an incompressible flow, $P = 0$, $Q = (W_{ij}W_{ij} - S_{ij}S_{ji})/2$, and $R = (-S_{ij}S_{jk}S_{ki} - 3W_{ij}W_{jk}W_{ki})/3$. Since Q is relevant to both local enstrophy and local strain or energy dissipation rate, and can reflect not only the rotation intensity but also the deformation intensity of the fluid element, the basic idea of the Q method is to extract the vortex tubes by identifying regions where the second invariant $Q > 0$.

There are fewer methods for identifying vortex sheet structures in turbulent flows compared to that for vortex tube structures due to the unsteadiness of the vortex sheet. We adopt a method proposed by Horiuti and Takagi[49] to extract vortex sheets in our simulated FHIT. Creating a symmetric tensor using the strain tensor $\boldsymbol{S}$ and the vorticity tensor $\boldsymbol{W}$, $\boldsymbol{A} = \boldsymbol{SW} + \boldsymbol{WS}$, and because of $A_{ii} = 0$, the equation of its eigenvalue, x, is written as

$$x^3 - (A_{ij}A_{ji})x/2 - A_{ij}A_{jk}A_{ki}/3 = 0. \tag{20}$$

Then, $[A_{ij}]_z$, $[A_{ij}]_+$, and $[A_{ij}]_-$ are used to represent the eigenvalues whose eigenvectors are the most parallel to the velocity vector, the largest, and smallest in the remaining eigenvalues, respectively. The identification of vortex sheet structures is by the criterion

$$[A_{ij}]_+ > \{[A_{ij}]_+\}_{th}, \tag{21}$$

where $\{[A_{ij}]_+\}_{th}$ is an arbitrary threshold value.

The extracted vortex tube and sheet structures in the FHIT for both Newtonian fluid and polymer solution cases are

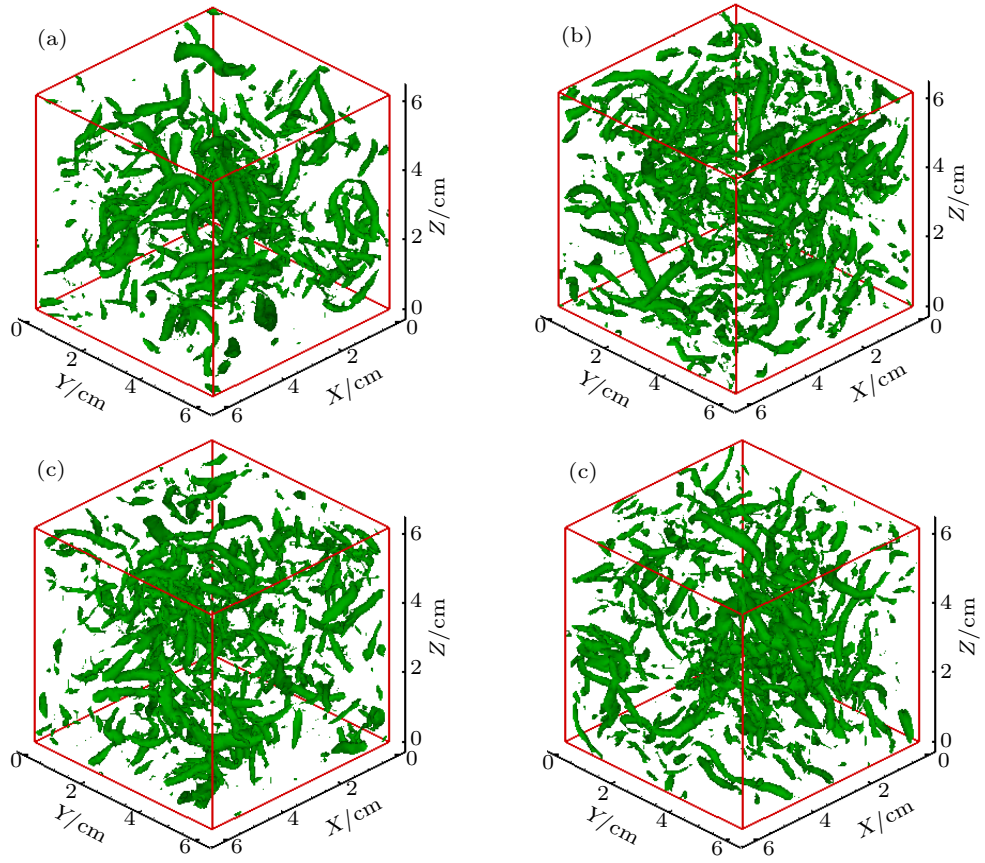


Fig. 9. (color online) Constant Q isosurfaces ($Q = 20$) for extracting vortex tube structures at $t = 80$ s for (a) Newtonian fluid case and polymer solution cases at (b) $Wi = 0.357$, $\beta = 0.6$; (c) $Wi = 0.357$, $\beta = 0.8$; and (d) $Wi = 0.857$, $\beta = 0.8$.

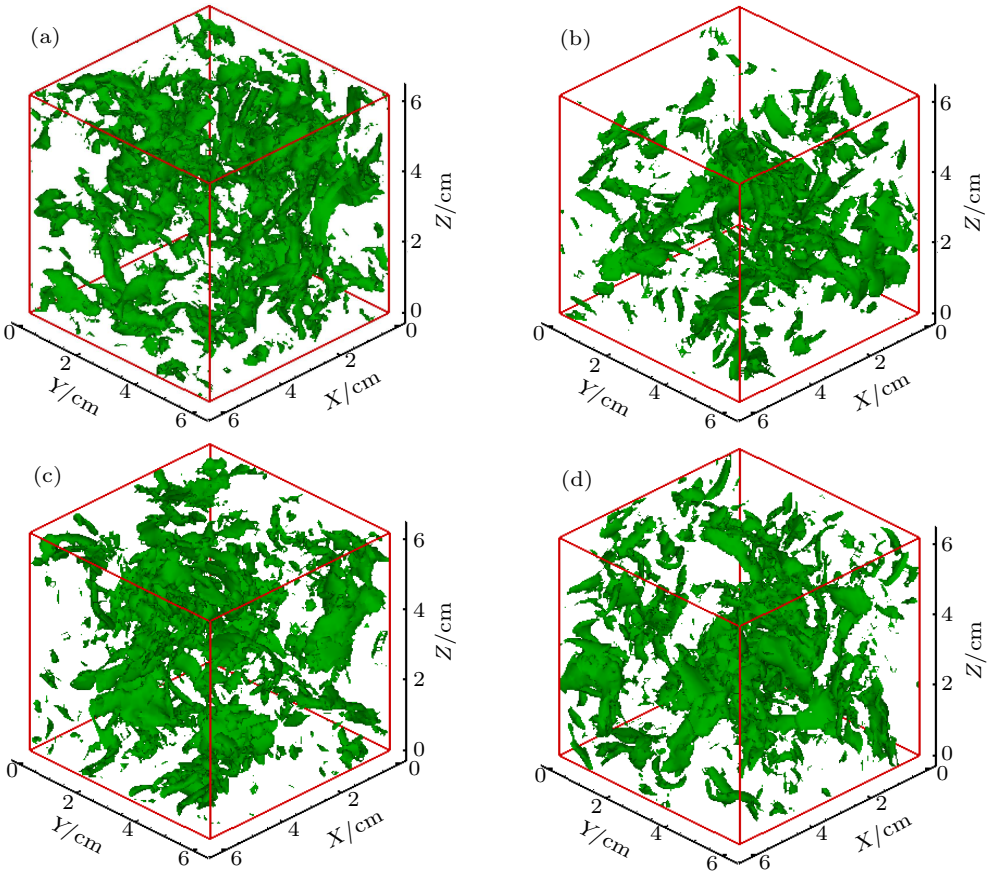


Fig. 10. (color online) Constant $[A_{ij}]_+$ isosurfaces ($[A_{ij}]_+ = 35$) for extracting vortex tube structures at $t = 80$ s for (a) Newtonian fluid case and polymer solution cases at (b) $Wi = 0.357$, $\beta = 0.6$; (c) $Wi = 0.357$, $\beta = 0.8$; and (d) $Wi = 0.857$, $\beta = 0.8$.

shown in Figs. 9 and 10, respectively. It is seen from Fig. 9 that the amount of vortex tubes in the polymer solution flow becomes apparently less than that in the Newtonian fluid flow, and decreases with the decrease of β. This indicates the decrease of enstrophy caused by viscoelasticity, which is in accordance with the strain (half of enstrophy) shown in Figs. 5(a) and 6. Since the vortex tube structures are closely related to the intermittent characteristics of turbulence as mentioned above, Fig. 9 also indicates that the addition of polymers restrains the turbulence intermittency (as depicted later). Within the limited range of currently simulated Wi, the influence of Wi on the vortex tube structures is not obvious (see Figs. 9(c) and 9(d)). The vortex sheet structures show a similar phenomenon as the vortex tubes as shown in Fig. 10, i.e., the vortex sheets are also inhibited in the polymer solution flow compared with that in the Newtonian fluid flow, and the inhibition is more serious at a denser polymer solution concentration. In a nutshell, the addition of polymer additives restrains both vortex tube and vortex sheet structures, and decreases the turbulent energy dissipation rate (see Fig. 3(d)).

3.3. Turbulence intermittency in FHIT influenced by polymer additives

From both spatial and temporal viewpoints, the turbulence is a nonlinear phenomenon containing coherent structures, which results in the intermittent characteristics. The extracted vortex structures indirectly suggest the occurrence of intermittency. Quantitative analyses of the small-scale intermittency in the FHIT of both the Newtonian fluid and the polymer solution cases are performed with the consideration of high-order velocity derivative correlations, such as the skewness and flatness factors. The expression of the high-order velocity derivative correlation is

$$F_{\partial u^n} = \frac{\left\langle \left(\frac{\partial u}{\partial x}\right)^n \right\rangle}{\left\langle \left(\frac{\partial u}{\partial x}\right)^2 \right\rangle^{\frac{1}{2}n}}, \tag{22}$$

where $\langle \cdots \rangle$ is the operation of the ensemble average. When $n = 3$, $F_{\partial u^3}$ becomes the skewness (or $S_{\partial u}$), and $F_{\partial u^4}$ is the flatness when $n = 4$. For a Gaussian distribution of the fluctuating velocity field, $F_{\partial u^3} = 0$ and $F_{\partial u^4} = 3$. The $F_{\partial u^3}$ reflects the asymmetry appearance on the PDF profile of random variables in turbulent flows and the nonlinearity in the Navier–Stokes equation. It also represents the production rate of vorticity by vortex stretching, and is closely related to the turbulent energy dissipation rate. The $F_{\partial u^4}$ represents the small-scale intermittency in turbulence. For the Newtonian fluid and the polymer solution cases, $F_{\partial u^3}$ and $F_{\partial u^4}$ are computed and shown in Table 2.

From Table 2, it can be found that $F_{\partial u^3}$ for all cases are close to -0.5, implying that the velocity gradient fields in the FHIT for both the Newtonian fluid and the polymer solution cases are obviously asymmetrical. For both the Newtonian fluid and the polymer solution cases, $F_{\partial u^4}$ is larger than 3, representing the existence of small-scale intermittency in the FHIT. The flatness factors in the FHIT of polymer solutions are all lower than those for the Newtonian fluid case, indicating that the small-scale intermittency is inhibited by the addition of polymers.

Table 2. Skewness and flatness factors of velocity derivatives.

	$F_{\partial u^3}(S_{\partial u})$	$F_{\partial u^4}$
Newtonian fluid	−0.4283	4.8654
$Wi = 0.357$, $\beta = 0.6$	−0.4568	4.7735
$Wi = 0.357$, $\beta = 0.7$	−0.4680	4.7738
$Wi = 0.357$, $\beta = 0.8$	−0.4410	4.6595
$Wi = 0.357$, $\beta = 0.9$	-0.4307	4.6736
$Wi = 0.357$, $\beta = 0.95$	−0.4281	4.6710
$Wi = 0.857$, $\beta = 0.8$	−0.4536	4.7453
$Wi = 0.857$, $\beta = 0.9$	−0.4337	4.7074
$Wi = 0.857$, $\beta = 0.95$	−0.4237	4.6209

Furthermore, we explore the intermittency at different scales using the discrete wavelet transform (DWT) approach. There are many kinds of models for the DWT. Daubechies not only proved the existence of orthonormal bases of compactly supported wavelets and constructed them (so-called Daubechies wavelet),[50] but also provided the well-done Daubechies wavelet bases for the first time.[51] In Daubechies wavelet, the smoothness of the scaling and the wavelet functions can be improved by increasing the vanishing moment. However, the computation cost is also increased with the increase of the vanishing moment. In this paper, we use the Daubechies wavelet with three-order vanishing moment to decompose data into 15 scales (the scale is 2^n). The definition of flatness factor for different scales in the DWT is

$$\mathrm{FF}(a) = \frac{\langle |W(a,t)|^4 \rangle_t}{\langle |W(a,t)|^2 \rangle_t^2}, \tag{23}$$

where $\langle \cdots \rangle_t$ is the time average between $t = 15$ s and $t = 120$ s for 105,000 sampling points with the interval time 0.001 s (after LES reaching statistically steady state); and $W(a,t)$ is the wavelet coefficient for different scale a. The flatness factors of the streamwise velocity fluctuations in the FHIT for Newtonian fluid and polymer solution cases are plotted in Fig. 11. It can be seen that the intermittency exists at all scales, and the flatness factor gradually decreases with increasing scale a. Overall, for the polymer solution flow, the flatness factor is slightly lower than that for the Newtonian fluid case. The same as that observed in the analysis of high-order velocity derivative correlations, it indicates that the small-scale intermittency is restrained by polymers. Figure 11 also shows that the flatness factors deviate from 3 before scale 2^{10} and the deviation increases with the decrease of the scale, implying that there exists stronger intermittency at smaller scales.

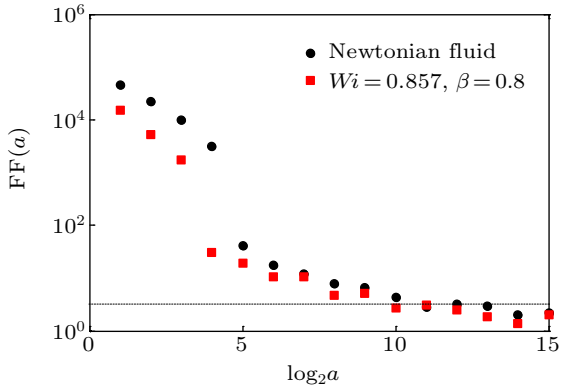


Fig. 11. (color online) Flatness factors of streamwise velocity fluctuations for different scales in DWT.

The above analyses of small-scale intermittency are based on fluctuating velocity fields. We also investigate the intermittency based on some other physical quantities. Siggia[52] proposed that all four-order velocity derivative correlations in HIT can be expressed by four rotational invariants consisting of the velocity-strain tensor and the vorticity tensor

$$I_1 = \langle S^4 \rangle,\ I_2 = \langle W^2 S^2 \rangle,\ I_3 = \langle W_i S_{ij} S_{jk} W_k \rangle,\ I_4 = \langle W^4 \rangle, \quad (24)$$

where $S^2 = \sum S_i^2$, $S^4 = (S^2)^2$, and $W^2 = \sum W_i^2$. Then these four correlations are normalized into dimensionless values as follows:

$$F_1 = \frac{15}{7}\frac{I_1}{\langle S^2 \rangle^2},\ F_2 = 3\frac{I_2}{\langle W^2 \rangle \langle S^2 \rangle},$$
$$F_3 = 3\frac{I_3}{\langle W^2 \rangle \langle S^2 \rangle},\ F_4 = \frac{9}{5}\frac{I_4}{\langle W^2 \rangle^2}. \quad (25)$$

In Eq. (25), F_1 is the flatness factor of energy dissipation rate or strain; F_2 and F_3 represent the relationship between strain and vorticity; and F_4 is the flatness factor of enstrophy or vorticity. These four parameters for the Newtonian fluid and the polymer solution flows are shown in Table 3. It can be seen that the four rotational invariants in the polymer solution cases are all lower than that in the Newtonian fluid case. The F_4 is always larger than F_1 for both the Newtonian fluid and the polymer solution flows, indicating that the vorticity field has stronger intermittency than the strain field in both the Newtonian fluid and the polymer solution flows.

Table 3. Four rotational invariants.

	F_1	F_2	F_3	F_4
Newtonian fluid	4.7926	5.5077	0.2759	6.7519
$Wi = 0.357, \beta = 0.6$	4.7769	5.5040	0.2555	6.6888
$Wi = 0.357, \beta = 0.7$	4.7256	5.4107	0.2608	6.6333
$Wi = 0.357, \beta = 0.8$	4.6183	5.2342	0.2635	6.4462
$Wi = 0.357, \beta = 0.9$	4.6259	5.1915	0.2728	6.3975
$Wi = 0.357, \beta = 0.95$	4.6192	5.1642	0.2752	6.4100
$Wi = 0.857, \beta = 0.8$	4.6805	5.3092	0.2705	6.4804
$Wi = 0.857, \beta = 0.9$	4.6544	5.2197	0.2718	6.4205
$Wi = 0.857, \beta = 0.95$	4.5955	5.1521	0.2707	6.3353

3.4. Turbulence scaling law of the FHIT with polymer additives

The statistical properties of turbulence small scales can be described by the distribution of velocity increment $\delta \boldsymbol{u}(r) = \boldsymbol{u}(x+r) - \boldsymbol{u}(x)$, where $\boldsymbol{u}(x+r)$ and $\boldsymbol{u}(x)$ are the velocities along the x axis within r interval. The p-th order velocity increment is called the p-th order structure function

$$S_p(r) = \langle |\delta \boldsymbol{u}(r)|^p \rangle = \langle |\boldsymbol{u}(x+r) - \boldsymbol{u}(x)|^p \rangle. \quad (26)$$

In the inertial range $\eta \le r \le L$ (η is the Kolmogorov scale, $\eta = (\upsilon^3/\varepsilon)^{1/4}$), the modified Kolmogorov scaling law has the following form:

$$S_p(r) \propto r^{\zeta(p)}. \quad (27)$$

For the original Kolmogorov theory (K41 scaling law) without considering turbulence intermittency, $\zeta(p) = p/3$.

Equation (27) is only suitable for turbulence in high-Reynolds-number flows. Benzi *et al.*[53] came up with a kind of scaling law named the extended self-similarity (ESS), which is valid not only for high-Reynolds-number turbulent flows but also valid for moderate- and low-Reynolds-number turbulent flows, and has an extended suitable range of scale. The ESS has the following form:

$$S_p(r) \propto S_q(r)^{\zeta(p)/\zeta(q)}. \quad (28)$$

Since in the K41 scaling law, $\zeta(3) = 1$, $q = 3$ is usually adopted for the ESS

$$S_p(r) \propto S_3(r)^{\zeta(p)}. \quad (29)$$

For turbulent drag-reducing flows by additives, although a vanishing Reynolds shear stress phenomenon has been reported in some experimental studies on the turbulent drag-reduced wall-bounded flow (e.g., Refs. [54] and [55]), it is still at the turbulent flow state due to the non-zero intensity of velocity fluctuations, the appearance of turbulent bursting events, and the existence of turbulent coherent structures. Being still at the turbulent state, the drag-reducing flows by additives should also satisfy some kind of scaling laws. In our previous paper,[37] for the first time, we investigated the scaling properties of the velocity structure functions for a turbulent drag-reducing flow in an ESS manner. In that study, the ESS analysis was performed using a DNS database of a low-Reynolds-number FHIT with polymer additives, and it was obtained that, within the range of DNS-simulated Reynolds number ($Re_\lambda \approx 46$) and Weissenberg number, the scaling law of turbulence in a fashion of ESS in the FHIT with polymer additives shows similar characteristics to that of the Newtonian fluid case. The scaling properties are also investigated for the currently LES-simulated drag-reducing FHIT at the Reynolds number around two times ($Re_\lambda \approx 90$) higher than that in the previous DNS study. We first show $S_3(r)$ versus r/η in a log–log plot, as shown in Fig. 12. It can be clearly seen that the inertial range at which $S_3(r) \propto r$ for the polymer solution flows becomes narrower than that for the Newtonian

fluid flow. Also, at very small scales ($r < \eta$), the velocity difference is regular ($\delta \boldsymbol{u}(r) \propto r$) for both the Newtonian fluid and the polymer solution cases.

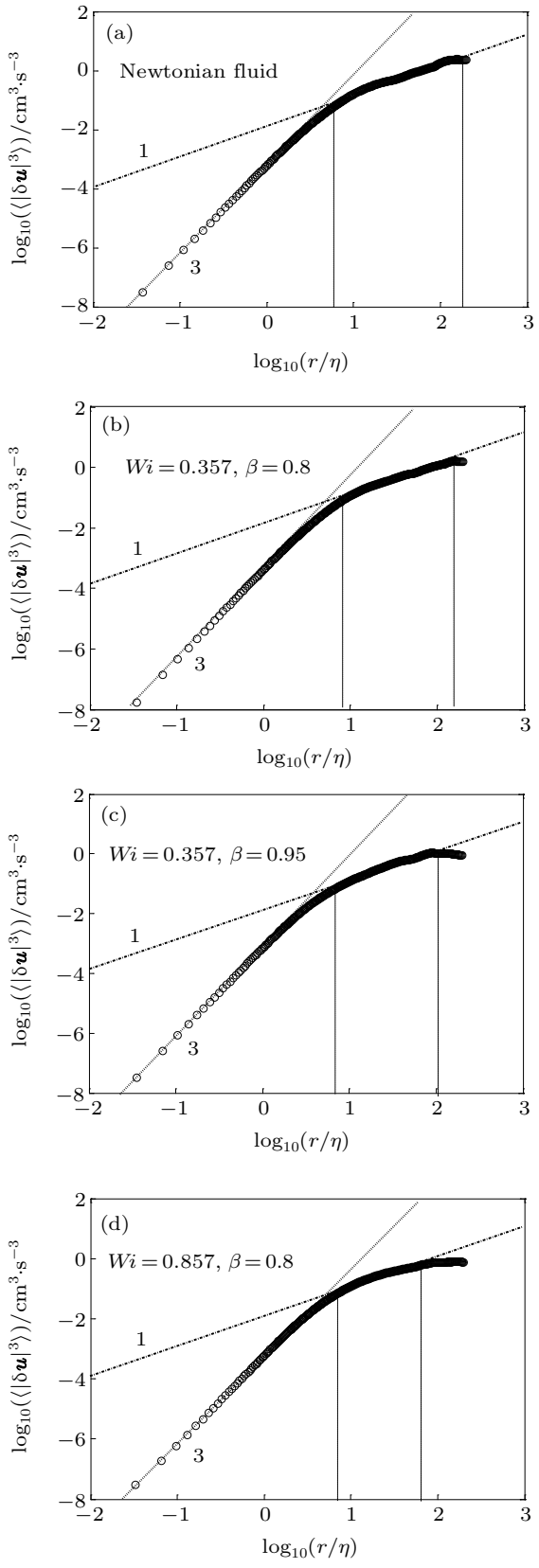


Fig. 12. Log–log plot of $S_3(r)$ versus r/η for (a) the Newtonian fluid case and polymer solution cases at (b) $Wi = 0.357$, $\beta = 0.8$; (c) $Wi = 0.357$, $\beta = 0.95$; and (d) $Wi = 0.857$, $\beta = 0.8$.

Then the relationship between $S_p(r)$ and $S_3(r)$ for both the Newtonian fluid and the polymer solution flows is explored in a fashion of ESS, as shown in Fig. 13. It shows that the addition of polymers has a nonvisible effect on the scaling law of the simulated FHIT, which is the same as that observed in our previous DNS study. To clarify that either this phenomenon is the truth for the turbulent drag-reducing flows by additives or it is due to the limited ranges of the simulated Wi and/or Re_λ calls for further studies.

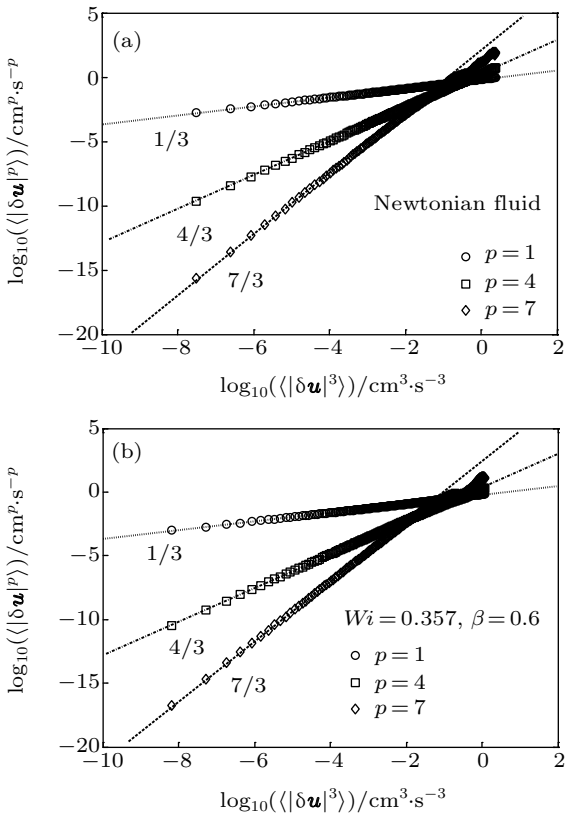


Fig. 13. Log–log plot of $S_p(r)$ versus $S_3(r)$ for (a) the Newtonian fluid case and (b) the polymer solution case at $Wi = 0.357$, $\beta = 0.6$.

4. Conclusions

LES studies of the FHIT in the Newtonian fluid and the polymer solutions based on the TADM have been carried out. It is verified that the TADM is a suitable SGS model for LES to simulate the turbulent drag-reducing FHIT in a viscoelastic turbulence. The LES and the DNS results are in good agreements for validation cases of the FHIT of the Newtonian fluid and the polymer solution. Analyses of statistical and structural characteristics and the scaling law of the FHIT with polymer additives have been conducted based on the LES database.

It is observed that the characteristics of the FHIT are remarkably altered by the addition of polymers. With the increases of the polymer solution concentration and Wi, the Taylor micro-scale and the turbulent integral scale in the FHIT are increased, and the turbulent kinetic energy and the energy dissipation rate are decreased. Both strain and vorticity in the

FHIT of the polymer solution are obviously lower than those in the Newtonian fluid case. In addition, the polymers can reduce the regions of large strain/vorticity but augment the regions of small strain/vorticity. The turbulent DR is obtained in the FHIT without the wall effect. The DR rate is increased with the increase of the polymer solution concentration and Wi. The extracted coherent structures, i.e., vortex tube and sheet, visually show that the turbulence in the FHIT with polymer additives is significantly suppressed as compared with that in the Newtonian fluid case. The inhibition of turbulent intermittency by polymer additives has been quantitatively analyzed by calculating the flatness factor at different scales based on the DWT method as well as the flatness factor of the velocity derivatives. The ESS scaling law has been investigated for the FHIT in both the Newtonian fluid and the polymer solution flows. Within the simulated ranges of Re_λ and Wi, the addition of polymers has a nonvisible effect on the scaling law of the simulated FHIT in a fashion of ESS. Further studies are necessitated to clarify whether this phenomenon is true for the turbulent drag-reducing flows by additives or occurs due to the limited ranges of the simulated Wi and/or Re_λ.

References

[1] Toms B A 1949 *Proceedings of the First International Congress of Rheology* (Amsterdam: North Holland) p. 135
[2] Burger E D, Munk W R and Wahl H A 1982 *J. Pet. Technol.* **34** 377
[3] Walker D T and Tiederman W G 1990 *J. Fluid Mech.* **218** 377
[4] Bewersdorff H W and Ohlendorf D 1988 *Colloid. Polym. Sci.* **266** 941
[5] Virk P S, Merrill E W, Mickley H S, Smith K A and Molo-Christensen E L 1967 *J. Fluid Mech.* **30** 305
[6] Zakin J L, Liu B and Bewersdorff H W 1998 *Rev. Chem. Eng.* **14** 253
[7] Hellsten M 2002 *J. Surfactants. Deterg.* **4** 65
[8] Li F C, Yu B, Wei J J and Hishida K 2008 *Int. J. Heat Mass Transfer* **51** 835
[9] Li F C, Kawaguchi Y, Segawa T and Hishida K 2005 *Phys. Fluids* **17** 075104
[10] Li F C, Kawaguchi Y, Hishida K and Oshima M 2006 *Exp. Fluids* **40** 218
[11] Aguilar G, Gasljevic K and Matthys E F 1999 *J. Heat Transfer* **121** 796
[12] Wei J J, Kawaguchi Y, Li F C, Yu B, Zakin J L, Hart D J and Zhang Y 2009 *Int. J. Heat Mass Transfer* **52** 3547
[13] Cai W H, Li F C, Zhang H N, Li X B, Yu B, Wei J J, Kawaguchi Y and Hishida K 2009 *Phys. Fluids* **21** 115103
[14] Sureshkumar R, Beris A N and Handler R A 1997 *Phys. Fluids* **9** 743
[15] Dimitropoulos C D, Sureshkumar R and Beris A N 1998 *J. Non-Newtonian Fluid Mech.* **79** 433
[16] Ptasinski P K, Boersma B J, Nieuwstadt F T M, Hulsen M A, Van den Brule B H A A and Hunt J C R 2003 *J. Fluid Mech.* **490** 251
[17] Li C F, Gupta V K, Sureshkumar R and Khomami B 2006 *J. Non-Newtonian Fluid Mech.* **139** 177
[18] Min T, Yoo J Y, Choi H and Joseph D D 2003 *J. Fluid Mech.* **486** 213
[19] Tamano S, Itohm M, Hoshizaki K and Yokota K 2007 *Phys. Fluids* **19** 075106
[20] Cai W H, Li F C and Zhang H N 2011 *Chin. Phys. B* **20** 124702
[21] Cruz D O A and Pinho F T 2003 *J. Non-Newtonian Fluid Mech.* **144** 109
[22] Cruz D O A, Pinho F T and Resende P R 2004 *J. Non-Newtonian Fluid Mech.* **121** 127
[23] Smagorinsky J 1963 *Mon. Weather Rev.* **91** 99
[24] Germano M, Piomelli U, Moin P and Cabot W H 1991 *Phys. Fluids A* **3** 1760
[25] Bardina J 1983 *Improved Turbulence Models Based on Large Eddy Simulation of Homogeneous, Incompressible, Turbulent Flows* (Ph. D. dissertation) (Stanford: Stanford University)
[26] Domaradzki J A and Saiki E M 1997 *Phys. Fluids* **9** 2148
[27] Stolz S and Adams N A 1999 *Phys. Fluids* **11** 1699
[28] Stolz S, Adams N A and Klesiser L 2001 *Phys. Fluids* **13** 997
[29] Stolz S, Adams N A and Klesiser L 2001 *Phys. Fluids* **13** 2985
[30] Pruett C D 2000 *AIAA J.* **38** 1634
[31] Pruett C D, Thomas B C, Grosch C E and Gatski T B 2006 *Phys. Fluids* **18** 028104
[32] Thais L, Tejada-Martinez A E, Gatski T B and Mompean G 2010 *Phys. Fluids* **22** 013103
[33] Gotoh T, Fukayama D and Nakano T 2002 *Phys. Fluids* **14** 1065
[34] Rogallo R S 1981 *Technical Report No.* 81315, NASA
[35] van Doorn E, White C M and Sreenivasan K R 1999 *Phys. Fluids* **11** 2387
[36] Praud O, Fincham A M and Sommeria J 2005 *J. Fluids Mech.* **522** 1
[37] Cai W H, Li F C and Zhang H N 2010 *J. Fluids Mech.* **665** 334
[38] Li F C, Cai W H, Zhang H N and Wang Y 2012 *Chin. Phys. B* **21** 114701
[39] Vaithianathan T and Collins L R 2003 *J. Comput. Phys.* **187** 1
[40] Vaithianathan T, Robert A, Brasseur J G and Collins L R 2006 *J. Non-Newtonian Fluid Mech.* **140** 3
[41] Chen S Y, Doolen G D, Kraichnan R H and She Z S 1993 *Phys. Fluids* **5** 458
[42] Kline S J 1967 *J. Fluid Mech.* **30** 741
[43] Min T, Yoo J Y and Choi H 2001 *J. Non-Newtonian Fluid Mech.* **100** 27
[44] Siggia E D 1981 *J. Fluid Mech.* **107** 375
[45] Douady S, Couder Y and Brachet M E 1991 *Phys. Rev. Lett.* **67** 983
[46] Hunt J C R, Wray A and Moin P 1988 *Center for Turbulence Research* **CTR-S88** 193
[47] Dubief Y and Delcayre F 2000 *J. Turbulence* **1** 1
[48] Chakraborty P, Balachandar S and Adrian R J 2005 *J. Fluid Mech.* **535** 185
[49] Horiuti K and Takagi Y 2005 *Phys. Fluids* **17** 1
[50] Daubechies I 1988 *Commun. Pur. Appl. Math.* **41** 909
[51] Daubechies I 1992 *Ten Lectures on Wavelet* (1st edn.) (Philadelphia: Society for Industrial and Applied Mathematics) p. 194
[52] Siggia E D 1981 *Phys. Fluids* **24** 1934
[53] Benzi R, Ciliberto S, Tripiccione R, Baudet C, Massaioli F and Succi S 1993 *Phys. Rev. E* **48** R29
[54] Wei T and Willmarth W W 1989 *J. Fluid Mech.* **204** 57
[55] Kawaguchi Y, Segawa T, Feng Z P and Li P W 2002 *Int. J. Heat Fluid Flow* **23** 700